

Cite as: P. Martínez-Garzón *et al.*, *Science*  
10.1126/science.adz0072 (2025).

# Progressive eastward rupture of the Main Marmara fault toward Istanbul

Patricia Martínez-Garzón<sup>1,2\*</sup>, Xiang Chen<sup>3</sup>, Dirk Becker<sup>4</sup>, Sebastián Núñez-Jara<sup>1</sup>, Recai Feyiz Kartal<sup>5</sup>, Elif Türker<sup>1</sup>, Georg Dresen<sup>1,6</sup>, Yehuda Ben-Zion<sup>7,8</sup>, Jorge Jara<sup>1</sup>, Fabrice Cotton<sup>1,6</sup>, Filiz Tuba Kadirioglu<sup>5</sup>, Tuğbay Kılıç<sup>5</sup>, Marco Bohnhoff<sup>1,9</sup>

<sup>1</sup>Helmholtz Centre Potsdam GFZ German Research Centre for Geosciences, Potsdam, Germany. <sup>2</sup>RWTH University of Aachen, Aachen, Germany. <sup>3</sup>Ruhr-University of Bochum, Bochum, Germany. <sup>4</sup>University of Hamburg, Hamburg, Germany. <sup>5</sup>AFAD Disaster and Emergency Management Presidency, Ankara, Türkiye. <sup>6</sup>Institute of Geosciences, University of Potsdam, Potsdam, Germany. <sup>7</sup>Faculty of Geosciences, University of Southern California, Los Angeles, CA, USA. <sup>8</sup>California State-Wide Earthquake Center, Los Angeles, CA, USA. <sup>9</sup>Free University Berlin, Institute of Geological Sciences, Berlin, Germany.

\*Corresponding author. Email: patricia@gfz.de

**The Main Marmara fault (MMF) in northwestern Türkiye poses the highest seismic risk in broader Europe. The 2025  $M_w$  6.2 was the largest earthquake along the MMF in >60 years. We integrated observations from multiple temporal scales including the decade-long evolution of  $M > 5$  earthquakes, their rupture dynamics and aftershock patterns. We show a series of eastward propagating  $M > 5$  events and a gradual eastward partial rupture of the MMF over the last ~15 years. The seismically active portion of the fault includes creeping and transitional segments with some of the most recent seismicity located near the presumably locked Princes Islands segment south of Istanbul that has the potential to generate a  $M > 7$  earthquake. Our analysis highlights the necessity of real-time monitoring of this part of the MMF.**

It is generally assumed that earthquakes tend to nucleate in areas where shear stress exceeds strength and their ruptures propagate until the flow of strain energy to the tip becomes too small to overcome local fracture strength. On heterogeneous faults, earthquake ruptures are primarily controlled by the stress distribution along the fault and will propagate toward regions with reduced normal stress or enhanced shear stress (1, 2). This behavior is supported by numerical models of earthquake nucleation on rough faults (3) and experimental work (4, 5). Stress may be concentrated locally at structural heterogeneities such as fault junctions, fault bends, or boundaries between regions of seismic and aseismic slip (6). Earthquake ruptures may also be affected by the elastic properties across the fault surface. The presence of bimaterial interfaces changes the normal stress across the fault during earthquake ruptures and may impact the rupture propagation direction and stress transfer to the surrounding regions (7, 8).

The Sea of Marmara in northwest Türkiye represents the most prominent hot spot for seismic hazard and risk in broader Europe (9). This region includes the western end of the North Anatolian Fault Zone (NAFZ), a major active transform plate boundary with a right-lateral slip rate of the Anatolian plate, with respect to the Eurasian plate, amounting to 17–29 mm/yr (10, 11). Most of the ~1200-km-long NAFZ has ruptured in a sequence of westward migrating  $M > 7$  earthquakes during the 20th century, leaving the Sea of Marmara segment, referred to here as the Main Marmara fault (MMF), largely unbroken (12). One cause for the westward epicenter propagation is stress transfer from previous earthquakes,

which loads the edges of the ruptured segments (13). Historical earthquake records for the segments near Istanbul (population > 18 million) date back 2,300 years and highlight multiple  $M > 7$  earthquakes, with the last three occurring along the Avcılar segment in 1509, at Princes Islands in 1766 and in the Gulf of Izmit in 1894 (14, 15). Based on macroseismic data, magnitudes for these earthquakes are estimated to be in the range of  $M_s$  6.8 to 7.3 (14, 15). Previous studies have reported an aggregated 30-year Poisson probability of  $M > 7.3$  earthquakes near Istanbul of 35%, which increases to 47% if time dependence and stress transfer from the 1999 Izmit earthquake are considered (16).

In this study, we jointly analyzed the rupture characteristics of the 23 April 2025  $M_w$  6.2 Marmara earthquake and the regional seismicity pattern during the last decades using a consistent seismicity catalog covering almost 20 years. The Marmara earthquake ruptured ~10–20 km of the central MMF, derived from scaling laws (17) and the extent of the early aftershock distribution (Fig. 1D). It ruptured with strike-slip kinematics, consistent with the E–W trending geometry of the MMF. This earthquake partially overlapped the ~10 km rupture of the 2019  $M_w$  5.8 Silivri earthquake (18, 19). Rupture kinematics of the 2019 earthquake may have involved secondary strike-slip and reverse faults (20) and likely transferred co-seismic static stress to the  $M_w$  6.2 rupture segment (19, 21).

The 2025 Marmara and 2019 Silivri earthquakes were the largest in the Sea of Marmara over the last 60 years. Based on the detection and analysis of earthquake repeaters across the region, the location of both epicenters marks the change

from the creeping Central Basin segment of the MMF to the transitional Kumburgaz Basin segment (Fig. 1A), where the occurrence of earthquake repeaters progressively tapers off (22). Immediately to the east, south of Istanbul, the MMF includes the locked Avclar and WNW–ESE-trending Princes Island segments (23, 24). Fault segments are stressed primarily from tectonic loading by plate motion and co-seismic and post-seismic stress transfer from previous earthquakes. Transitional fault segments become additionally loaded by strain release along neighboring creeping sections (25), resulting in higher stress concentrations (26).

### **Decade-long progressive partial rupturing of the Main Marmara fault from west to east**

We observed a pronounced eastward migration of  $M > 5$  events along the MMF during the last 15 years (Figs. 1, B to D), accompanied by a rough increase in magnitude over time. Eastward migration started on the creeping section (Western High and Central Basin segments as documented by seafloor geodesy (27), and numerous earthquake repeaters (22, 28, 29), Fig. 1A). This segment became active during 2011–2012 with two  $M > 5$  earthquakes leaving a ~10-km-long seismically quiet region at the eastern edge of the creeping segment (asperity marked by the orange arrow in Fig. 1B). This segment was then activated in 2019 when the  $M_w$  5.8 Silivri earthquake nucleated on a secondary structure connected to the MMF (Fig. 1C). Notably, the 2019  $M_w$  5.8 rupture occurred precisely within the zone that had remained quiet following the earlier  $M > 5$  events in 2011 and 2012 (Fig. 1B). Most recently, aftershocks of the 2025  $M_w$  6.2 Marmara earthquake terminated near the eastern edge of a ~15-km-long seismically quiet zone (Fig. 1D), mirroring the previously observed pattern for the 2011–2012 seismic sequence.

These observations document a recent eastward partial rupturing of the fault toward the locked segments south of western Istanbul (Fig. 1A). Ongoing aseismic deformation appears to be loading the transitional segment between the eastern edge of the Central Basin and Kumburgaz Basin), where the 2019  $M_w$  5.8 and 2025  $M_w$  6.2 earthquakes nucleated. The 2025  $M_w$  6.2 earthquake ruptured on this transitional zone and was arrested in a region that appears to be locked, based on measurements from seafloor geodesy (30) and the complete absence of seismic repeaters (22). However, the  $M_w$  6.2 event only released a minor portion (~20 cm from plausible co-seismic slip estimates (31)) of the estimated slip deficit (approximately 6 m if we assume 23 mm/yr) for this segment since the last large earthquake in 1766.

The reported eastward migration of  $M > 5$  events on the MMF over the last 15 years appears to be associated with a rough increase in magnitude from  $M_w$  5.1–5.2 to  $M_w$  6.2. Although we note that the number of available observations is limited, this could reflect a higher elastic strain accumulated

on the fault as the earthquakes have migrated from the creeping segments toward the locked segments. Alternatively, increasing magnitudes could also reflect rupture of larger asperities along the fault as it progressively weakens, smoothing the stress field at longer wavelengths and enabling earthquakes to propagate for longer distances (32) in a large-scale localization process (33, 34). These effects have also been observed in rock deformation experiments on rough faults (35).

### **Eastward rupture propagation of the 2019 $M_w$ 5.8 and 2025 $M_w$ 6.2 earthquakes**

We also investigated whether these events showed a predominant rupture direction, employing two approaches, i) measuring the duration of the initial P-waves for seismometers located at epicentral distances between 50 and 100 km as a function of azimuth and ii) measuring the azimuthal variation of peak ground-motion acceleration.

Variation in duration of the first-motion pulse from stations at comparable epicentral distances can be used to infer whether the earthquake displays rupture directivity. For both the 2025  $M_w$  6.2 and 2019  $M_w$  5.8 earthquakes, the P-wave first pulse had shorter durations at the stations located east of the epicenters, suggesting an eastward rupture directivity (Fig. 2 and fig S1). This agrees with the regional directivity pattern observed for most MMF  $M > 3.5$  earthquakes, particularly those occurring on western fault segments (36).

Rupture directivity can also be quantified by measuring azimuthal variations in ground-motion peak ground acceleration and velocities and then calculating residuals between observed motions and predictions from recent isotropic ground-motion models commonly used in engineering seismology (37). For both earthquakes, the residuals exhibited an azimuthal dependence (figs. S2 and S3), with larger values toward Izmit and the Armutlu Peninsula. This pattern also supports an eastward rupture propagation and associated directivity effects.

Rupture directivity promotes enhanced ground motion and damage potential in the forward direction, manifested for example in an asymmetric aftershock pattern with respect to the epicenter (38). This agrees with our observations for both the 2019 and 2025 mainshocks (Fig. 2 and figs. S1 and S2), which show an eastward distribution of aftershocks along the MMF (Fig. 2, A and B, and fig. S1). According to scaling relations, a strike-slip earthquake of  $M_w$  6.2 typically ruptures about 10–20 km (17, 31) which is smaller than the extent of the aftershocks to the east of the epicenter (extending for approximately 25 km during the first week after the mainshock, see Fig. 2).

### **MMF seismicity rates and *b*-value evolution (2015–2025)**

Due to the epicentral proximity of the 2025  $M_w$  6.2 and the

2019  $M_w$  5.8 earthquakes, we analyzed and compared the pre-, inter-, and post-seismic behavior of the seismicity from this region. We also investigated the temporal evolution of the seismicity and its magnitude-frequency distribution at various distances from the 2025  $M_w$  6.2 epicenter.

Near the epicenter (radius  $R < 30$  km), following the aftershock sequence of the 2019  $M_w$  5.8 earthquake, no significant event rate changes were observed (Fig. 3A) up until the 2025  $M_w$  6.2 sequence. The roughly constant event rate may suggest a stable fault loading process along the creeping section. This is similar to the period before the 2019  $M_w$  5.8 event, when stable event rates were episodically punctuated by small bursts of cascading activity.

The seismic  $b$ -value, reflecting the relation of larger to smaller events, is frequently assumed to be inversely correlated with stress level (39–41). Stress accumulation and enhanced damage have often been monitored before earthquakes by means of the  $b$ -value (41–44). We quantified the  $b$ -value evolution using the  $b$ -positive estimator (45). The  $b$ -positive evolution in the region  $R < 30$  km from the epicentral region shows a significant progressive decrease from about  $\sim 0.95 \pm 0.10$  in January 2015 down to  $0.70 \pm 0.10$  in 2019 before the  $M_w$  5.8 earthquake (Fig. 3). No comparable, quasi-continuous,  $b$ -value decrease in the 5 years before the  $M_w$  5.8 earthquake is observable beyond the  $R < 30$  km range.

High seismicity rates of aftershock sequences tend to increase the  $b$ -value. This has been utilized to monitor the evolution of seismic sequences and evaluate the potential for upcoming large earthquakes (46, 47). For the 2019  $M_w$  5.8 event,  $b$ -value increased during the early aftershock sequence and then progressively recovered to pre-mainshock values, significantly decreasing from  $\sim 1 \pm 0.1$  to  $0.8 \pm 0.1$  during the following two years, in agreement with the regional  $b$ -positive (Fig. 3, B and C). This correlates in time with decreasing event rates following the 2019  $M_w$  5.8 event, reaching a stable value by mid-2021. Combined, this could be interpreted as a stress relaxation/loading cycle as often observed in laboratory tests (48) and other earthquake sequences in nature (46, 47).

From the current catalog, the observed  $b$ -value pattern before and after the 2025  $M_w$  6.2 event is different from that of the  $M_w$  5.8 event. In the years before the  $M_w$  6.2 event, the local (radius  $R < 30$  km)  $b$ -value ( $0.85 \pm 0.15$ ) remained comparable to the regional value without further decrease (Fig. 3, B and D). Furthermore, the  $b$ -value related to the early 2025  $M_w$  6.2 aftershock sequence did not increase. Instead,  $b$ -value remained similar or slightly lower (within 95% confidence interval) than before the mainshock (Fig. 3D).

## Stress transfer from the 2019 $M_w$ 5.8 and 2025 $M_w$ 6.2 earthquakes and seismicity near the locked segments

The cumulative Coulomb stress transfer from the  $M_w$  5.8 and

$M_w$  6.2 earthquakes reaches up 0.2 MPa locally on the MMF, near the edges of the rupture where a large cluster of aftershocks has occurred (Fig. 4A). This value may decrease down to 0 MPa when modifying the source fault parameters (strike, dip, rake) up to  $10^\circ$  each (fig. S5). At the Avclar fault segment, between the Kumburgaz Basin and the western end of the Princes Islands segment, the stress transfer is estimated to be 0.05–0.1 MPa irrespective of small perturbations of the source fault (Fig. 4 and fig. S5).

The western end of the Princes Island segment has not experienced a significant (e.g.,  $>0.1$  MPa) static stress change from these earthquakes. However, the fault zone between the Avclar and the Princes Islands segments has hosted abundant seismicity during the last 15 years (purple box in Fig. 4A), including seismicity preceding and following the 2019  $M_w$  5.8 and 2025  $M_w$  6.2 events (Fig. 4B). This sensitive cluster delineates the western termination of the seismic gap along the northern rim of the Çinarcık basin (23).

## Outlook for MMF seismicity

The 2025  $M_w$  6.2 earthquake is the latest in a sequence of four  $M > 5$  earthquakes in the last 15 years progressively migrating eastward along the MMF and displaying roughly increasing magnitudes. These compose all the  $M > 5$  events that have occurred on the MMF since the 1999  $M_w$  7.4 Izmit earthquake. The last two events occur at the transition between the creeping Central Basin and the locked eastern fault segments. This decade-long eastward  $M > 5$  earthquake migration is consistent with the occurrence of  $M > 6.5$  historical earthquakes in the Sea of Marmara (14) and in contrast to the overall westward migration of  $M > 7$  earthquakes observed along the NAFZ to the east of the Sea of Marmara region during the 20th century (12). In addition to the 2025  $M_w$  6.2 event, other small and moderate earthquakes in the Sea of Marmara region have displayed a preferential eastward rupture propagation toward the locked Princes Islands segment immediately south of Istanbul (36, 37).

What is driving this pattern of eastward earthquake rupture propagation on the decadal and intra-event scales? We posit that the creeping fault section to the west (22, 27–29) may contribute to loading the locked MMF segment to the east (23, 24), causing progressive stress transfer and partial rupturing in a series of medium-sized events. The stress history from previous mainshocks increases the shear stress at the edges of previous ruptures and thus may promote an eastward event migration at the decadal scale. The observed rupture directivity could possibly be related to a velocity contrast across the fault, as has been observed elsewhere (e.g., (49)), although this has not yet been shown for the MMF. Independently of their driving factors, the persistent rupture directivity and enhanced ground motion to the east (Fig. 2 and (36)) are expected to also aid the stress transfer and

migration of earthquakes to the east.

What are the implications for future large earthquakes? Together with the previous earthquake ruptures on the Main Marmara Fault over the last decade, the  $M_w$  6.2 earthquake sequence leaves only a ~15–20 km-long region with low seismic activity in the Avcılar segment, between the Kumburgaz and the locked Princes Islands segment. As the 2019  $M_w$  5.8 seismic sequence began in a similarly quiet area, our results suggest that this seismically silent segment is a possible candidate for the next moderate to large earthquakes. This is likely connected to both the slow but continuous stress accumulation produced by the adjacent creeping and transitional segments acting on the locked portion of the fault, and the Coulomb stress transfer from the previous  $M > 5$  earthquakes. For future ruptures on the eastern part of the MMF, one possibility is the rupture of the remaining part of the transition segment between the 2025  $M_w$  6.2 earthquake and the western part of the locked Princes Island segment (Fig. 4). This segment is large enough to generate a future  $M \sim 6$  event, which would further increase the static stress on the locked Princes Island segment. The western edge of the Princes Island segment is also persistently active seismically (purple rectangle in Fig. 4). If the locked Princes Islands segment (Fig. 4) were to host a greater earthquake, the effects of eastward ground-motion directivity would impact Istanbul. It should be noted, however, that not all earthquakes along the same fault zone must display the same directivity pattern, as already observed e.g., in the Parkfield segment of the San Andreas Fault (e.g., (50)). In a plausible alternative scenario, a large earthquake might also initiate west of the 1999  $M_w$  7.4 Izmit rupture, to the east of the Princes Island segment. This scenario would be consistent with the westward propagation of major earthquakes from Eastern Türkiye to Izmit during the 20th century (12, 13).

Is the fault ready to rupture again? In the case of the 2019  $M_w$  5.8 earthquake, it took about 2 years for the  $b$ -value to recover to its local pre-seismic level. However, after the 2025  $M_w$  6.2 earthquake, the  $b$ -value did not increase locally as expected from an aftershock sequence, and it remained stable within the uncertainties around average local values. If the  $b$ -value for this sequence is representative of the stress level, this suggests that on this fault segment shear stress remained high (47).

What practical conclusions can be drawn from this analysis? This study highlights the emerging critical seismotectonic significance of the fault segment west of the locked Princes Islands section. Given the potential for continued eastward unlocking and the persistent seismicity localized at the Istanbul fault bend toward the Princes Islands segment, this portion of the fault could host the source of a future earthquake. Therefore, enhancing seismic monitoring systems along this submarine fault is of paramount importance,

and may require further borehole stations (in addition to those already existing, see (51)), permanent ocean bottom deployments and offshore fiber optic sensing across the MMF.

While the precise timing, location, magnitude, and rupture direction of a future major earthquake cannot be predicted with current knowledge, our present findings support previous research (36, 37) suggesting that seismic shaking in the eastern part of the Marmara Sea could be intensified by directivity effects if rupture propagates from west to east. These possible directivity effects should be incorporated into seismic risk assessments for the greater Istanbul area.

## REFERENCES AND NOTES

- R. Bürgmann, The geophysics, geology and mechanics of slow fault slip. *Earth Planet. Sci. Lett.* **495**, 112–134 (2018). doi:[10.1016/j.epsl.2018.04.062](https://doi.org/10.1016/j.epsl.2018.04.062)
- G. Calderoni, A. Rovelli, Y. Ben-Zion, R. Di Giovambattista, Along-strike rupture directivity of earthquakes of the 2009 L'Aquila, central Italy, seismic sequence. *Geophys. J. Int.* **203**, 399–415 (2015). doi:[10.1093/gji/ggv275](https://doi.org/10.1093/gji/ggv275)
- C. Cattania, P. Segall, Precursory Slow Slip and Foreshocks on Rough Faults. *J. Geophys. Res. Solid Earth* **126**, e2020JB020430 (2021). doi:[10.1029/2020JB020430](https://doi.org/10.1029/2020JB020430)
- E. Bayart, I. Svetlizky, J. Fineberg, Slippery but Tough: The Rapid Fracture of Lubricated Frictional Interfaces. *Phys. Rev. Lett.* **116**, 194301 (2016). doi:[10.1103/PhysRevLett.116.194301](https://doi.org/10.1103/PhysRevLett.116.194301) Medline
- Z. Reches, J. Fineberg, Earthquakes as Dynamic Fracture Phenomena (2023). <https://agupubs.onlinelibrary.wiley.com/doi/full/10.1029/2022JB026295>.
- J.-P. Avouac, From Geodetic Imaging of Seismic and Aseismic Fault Slip to Dynamic Modeling of the Seismic Cycle. *Annu. Rev. Earth Planet. Sci.* **43**, 233–271 (2015). doi:[10.1146/annurev-earth-060614-105302](https://doi.org/10.1146/annurev-earth-060614-105302)
- Y. Ben-Zion, D. J. Andrews, Properties and implications of dynamic rupture along a material interface. *Bull. Seismol. Soc. Am.* **88**, 1085–1094 (1998). doi:[10.1785/BSSA0880041085](https://doi.org/10.1785/BSSA0880041085)
- G. B. Brietzke, Y. Ben-Zion, Examining tendencies of in-plane rupture to migrate to material interfaces. *Geophys. J. Int.* **167**, 807–819 (2006). doi:[10.1111/j.1365-246X.2006.03137.x](https://doi.org/10.1111/j.1365-246X.2006.03137.x)
- H. Crowley, J. Dabbeek, V. Despotaki, D. Rodrigues, L. Martins, V. Silva, X. Romão, N. Pereira, G. Weatherill, L. Danciu, “European Seismic Risk Model (ESRM20)” (Report, ETH Zurich, 2021); <https://doi.org/10.7414/EUC-EFEHR-TR002-ESRM20>.
- A. A. Barka, The North Anatolian fault zone. *Annales Tectonicae* **6**, 164–195 (1992).
- T. Hergert, O. Heidbach, Slip-rate variability and distributed deformation in the Marmara Sea fault system. *Nat. Geosci.* **3**, 132–135 (2010). doi:[10.1038/ngeo739](https://doi.org/10.1038/ngeo739)
- A. M. C. Sengör, O. Tüysüz, C. İmren, M. Sakınç, H. Eyidoğan, N. Görür, X. Le Pichon, C. Rangin, The North Anatolian Fault: A new look. *Annu. Rev. Earth Planet. Sci.* **33**, 37–112 (2005). doi:[10.1146/annurev.earth.32.101802.120415](https://doi.org/10.1146/annurev.earth.32.101802.120415)
- R. S. Stein, A. A. Barka, J. H. Dieterich, “Progressive failure on the North Anatolian fault since 1939 by earthquake stress triggering” (United States Geological Survey, 1997); <https://pubs.er.usgs.gov/publication/70019873>
- N. Ambroseys, The Seismic Activity of the Marmara Sea Region over the Last 2000 Years. *Bull. Seismol. Soc. Am.* **92**, 1–18 (2002). doi:[10.1785/0120000843](https://doi.org/10.1785/0120000843)
- M. Bohnhoff, P. Martínez-Garzón, F. Bulut, E. Stierle, Y. Ben-Zion, Maximum earthquake magnitudes along different sections of the North Anatolian fault zone. *Tectonophysics* **674**, 147–165 (2016). doi:[10.1016/j.tecto.2016.02.028](https://doi.org/10.1016/j.tecto.2016.02.028)
- M. Murru, A. Akinci, G. Falcone, S. Pucci, R. Console, T. Parsons,  $M \geq 7$  earthquake rupture forecast and time-dependent probability for the sea of Marmara region, Turkey. *J. Geophys. Res. Solid Earth* **121**, 2679–2707 (2016). doi:[10.1002/2015JB012595](https://doi.org/10.1002/2015JB012595)
- M. Leonard, Self-Consistent Earthquake Fault-Scaling Relations: Update and Extension to Stable Continental Strike-Slip Faults. *Bull. Seismol. Soc. Am.* **104**, 2953–2965 (2014). doi:[10.1785/0120140087](https://doi.org/10.1785/0120140087)
- V. Durand, S. Bentz, G. Kwiatek, G. Dresen, C. Wollin, O. Heidbach, P. Martínez-Garzón, F. Cotton, M. Nurlu, M. Bohnhoff, A Two-Scale Preparation Phase Preceded an  $M_w$  5.8 Earthquake in the Sea of Marmara Offshore Istanbul, Turkey.

- Seismol. Res. Lett.* **91**, 3139–3147 (2020). doi:10.1785/0220200110
19. H. Karabulut, S. E. Güvercin, F. Eskiköy, A. Ö. Konca, S. Ergintav, The moderate size 2019 September Mw 5.8 Silivri earthquake unveils the complexity of the Main Marmara Fault shear zone. *Geophys. J. Int.* **224**, 377–388 (2021). doi:10.1093/gji/ggaa469
  20. F. Turhan, D. Acarel, V. Plicka, M. Bohnhoff, R. Polat, J. Zahradník, Coseismic Faulting Complexity of the 2019 Mw 5.7 Silivri Earthquake in the Central Marmara Seismic Gap, Offshore Istanbul. *Seismol. Res. Lett.* **94**, 75–86 (2022). doi:10.1785/0220220111
  21. M. Şahin, C. Yaltırak, F. Bulut, A. Garagon, Stress change generated by the 2019 İstanbul–Silivri earthquakes along the complex structure of the North Anatolian Fault in the Marmara Sea. *Earth Planets Space* **74**, 167 (2022). doi:10.1186/s40623-022-01706-2
  22. D. Becker, P. Martínez-Garzón, C. Wollin, T. Kılıç, M. Bohnhoff, Variation of Fault Creep Along the Overdue İstanbul–Marmara Seismic Gap in NW Türkiye. *Geophys. Res. Lett.* **50**, e2022GL101471 (2023). doi:10.1029/2022GL101471
  23. M. Bohnhoff, F. Bulut, G. Dresen, P. E. Malin, T. Eken, M. Aktar, An earthquake gap south of Istanbul. *Nat. Commun.* **4**, 1999 (2013). doi:10.1038/ncomms2999 Medline
  24. S. Ergintav, R. E. Reilinger, R. Çakmak, M. Floyd, Z. Çakır, U. Doğan, R. W. King, S. McClusky, H. Özener, İstanbul's earthquake hot spots: Geodetic constraints on strain accumulation along faults in the Marmara seismic gap. *Geophys. Res. Lett.* **41**, 5783–5788 (2014). doi:10.1002/2014GL060985
  25. S. T. Tse, R. Dmowska, J. R. Rice, Stressing of locked patches along a creeping fault. *Bull. Seismol. Soc. Am.* **75**, 709–736 (1985).
  26. R. A. Harris, Large earthquakes and creeping faults. *Rev. Geophys.* **55**, 169–198 (2017). doi:10.1002/2016RG000539
  27. R. Yamamoto, M. Kido, Y. Ohta, N. Takahashi, Y. Yamamoto, A. Pinar, D. Kalafat, H. Özener, Y. Kaneda, Seafloor Geodesy Revealed Partial Creep of the North Anatolian Fault Submerged in the Sea of Marmara. *Geophys. Res. Lett.* **46**, 1268–1275 (2019). doi:10.1029/2018GL080984
  28. M. Bohnhoff, C. Wollin, D. Domigall, L. Küperkoch, P. Martínez-Garzón, G. Kwiatek, G. Dresen, P. E. Malin, Repeating Marmara Sea earthquakes: Indication for fault creep. *Geophys. J. Int.* **210**, 332–339 (2017). doi:10.1093/gji/ggx169
  29. J. Schmittbuhl, H. Karabulut, O. Lengliné, M. Bouchon, Long-lasting seismic repeaters in the Central Basin of the Main Marmara Fault. *Geophys. Res. Lett.* **43**, 9527–9534 (2016). doi:10.1002/2016GL070505
  30. P. Sakić, H. Piété, V. Ballu, J.-Y. Royer, H. Kopp, D. Lange, F. Petersen, M. S. Özeren, S. Ergintav, L. Geli, P. Henry, A. Deschamps, No significant steady state surface creep along the North Anatolian Fault offshore Istanbul: Results of 6 months of seafloor acoustic ranging. *Geophys. Res. Lett.* **43**, 6817–6825 (2016). doi:10.1002/2016GL069600
  31. D. L. Wells, K. J. Coppersmith, New empirical relationships among magnitude, rupture length, rupture width, rupture area, and surface displacement. *Bull. Seismol. Soc. Am.* **84**, 974–1002 (1994). doi:10.1785/BSSA0840040974
  32. Y. Ben-Zion, M. Eneva, Y. Liu, Large earthquake cycles and intermittent criticality on heterogeneous faults due to evolving stress and seismicity. *J. Geophys. Res. Solid Earth* **108**, 2307 (2003). <https://doi.org/10.1029/2002JB002121>
  33. Y. Ben-Zion, I. Zaliapin, Localization and coalescence of seismicity before large earthquakes. *Geophys. J. Int.* **223**, 561–583 (2020). doi:10.1093/gji/ggaa315
  34. A. Kato, Y. Ben-Zion, The generation of large earthquakes. *Nat. Rev. Earth Environ.* **2**, 26–39 (2021). doi:10.1038/s43017-020-00108-w
  35. G. Kwiatek, P. Martínez-Garzón, T. Goebel, M. Bohnhoff, Y. Ben-Zion, G. Dresen, Intermittent Criticality Multi-Scale Processes Leading to Large Slip Events on Rough Laboratory Faults, Intermittent Criticality Multi-Scale Processes Leading to Large Slip Events on Rough Laboratory Faults. *J. Geophys. Res. Solid Earth* **129**, e2023JB028411 (2024). doi:10.1029/2023JB028411
  36. X. Chen, P. Martínez-Garzón, G. Kwiatek, Y. Ben-Zion, M. Bohnhoff, F. Cotton, Rupture Directivity of Moderate Earthquakes Along the Main Marmara Fault Suggests Larger Ground Motion Towards Istanbul. *Geophys. Res. Lett.* **52**, e2024GL111460 (2025). doi:10.1029/2024GL111460
  37. E. Türker, F. Cotton, M. Pilz, G. Weatherill, Analysis of the 2019 Mw 5.8 Silivri Earthquake Ground Motions: Evidence of Systematic Azimuthal Variations Associated with Directivity Effects. *Seismol. Res. Lett.* **93** (2A), 693–705 (2022). doi:10.1785/0220210168
  38. I. Zaliapin, Y. Ben-Zion, Asymmetric distribution of aftershocks on large faults in California. *Geophys. J. Int.* **185**, 1288–1304 (2011). doi:10.1111/j.1365-246X.2011.04995.x
  39. I. G. Main, P. G. Meredith, C. Jones, A reinterpretation of the precursory seismic b-value anomaly from fracture mechanics. *Geophys. J. Int.* **96**, 131–138 (1989). doi:10.1111/j.1365-246X.1989.tb05255.x
  40. C. H. Scholz, The frequency-magnitude relation of microfracturing in rock and its relation to earthquakes. *Bull. Seismol. Soc. Am.* **58**, 399–415 (1968). doi:10.1785/BSSA0580010399
  41. C. H. Scholz, On the Stress Dependence of the Earthquake b-value. *Geophys. Res. Lett.* **42**, 1399–1402 (2015). doi:10.1002/2014GL062863
  42. D. Amitrano, Brittle-ductile transition and associated seismicity: Experimental and numerical studies and relationship with the b value. *J. Geophys. Res. Solid Earth* **108**, 2044 (2003).
  43. D. Schorlemmer, S. Wiemer, M. Wyss, Variations in earthquake-size distribution across different stress regimes. *Nature* **437**, 539–542 (2005). doi:10.1038/nature04094 Medline
  44. W. D. Smith, The b-value as an earthquake precursor. *Nature* **289**, 136–139 (1981). doi:10.1038/289136a0
  45. N. van der Elst, B-positive: A Robust Estimator of Aftershock Magnitude Distribution in 384 Transiently Incomplete Catalogs. *J. Geophys. Res. Solid Earth* **126**, e2020JB021027 (2021). doi:10.1029/2020JB021027
  46. L. Giulia, S. Wiemer, E. Biondini, B. Enescu, G. Vannucci, Improving the Foreshock Traffic Light Systems for Real-Time Discrimination Between Foreshocks and Aftershocks. *Seismol. Res. Lett.* **95**, 3579–3592 (2024). doi:10.1785/0220240163
  47. L. Giulia, S. Wiemer, Real-time discrimination of earthquake foreshocks and aftershocks. *Nature* **574**, 193–199 (2019). doi:10.1038/s41586-019-1606-4 Medline
  48. T. H. Goebel, D. Schorlemmer, T. W. Becker, G. Dresen, C. G. Sammis, Acoustic emissions document stress changes over many seismic cycles in stick-slip experiments. *Geophys. Res. Lett.* **40**, 2049–2054 (2013). doi:10.1002/grl.50507
  49. A. A. Allam, Y. Ben-Zion, Seismic velocity structures in the Southern California plate-395 boundary environment from double-difference tomography. *Geophys. J. Int.* **190**, 1181–1196 (2012). doi:10.1111/j.1365-246X.2012.05544.x
  50. W. H. Bakun, B. Aagaard, B. Dost, W. L. Ellsworth, J. L. Hardebeck, R. A. Harris, C. Ji, M. J. S. Johnston, J. Langbein, J. J. Lienkaemper, A. J. Michael, J. R. Murray, R. M. Nadeau, P. A. Reasenberg, M. S. Reichle, E. A. Roeloffs, A. Shakal, R. W. Simpson, F. Waldhauser, Implications for prediction and hazard assessment from the 2004 Parkfield earthquake. *Nature* **437**, 969–974 (2005). doi:10.1038/nature04067 Medline
  51. M. Bohnhoff, G. Dresen, U. Ceken, F. T. Kadrioglu, R. F. Kartal, T. Kılıç, M. Nurlu, K. Yanık, D. Acarel, F. Bulut, H. Ito, W. Johnson, P. E. Malin, D. Mencin, GONAF—the borehole Geophysical Observatory at the North Anatolian Fault in the eastern Sea of Marmara. *Sci. Drill.* **22**, 19–28 (2017). doi:10.5194/sd-22-19-2017
  52. D. Becker, P. Martínez-Garzón, C. Wollin, T. Kılıç, M. Bohnhoff, Homogenized regional seismicity catalogue for the Marmara region, northwestern Turkey, for the time interval 2006–2020, version 1.0, GFZ Data Services (2023); <https://doi.org/10.5880/GFZ.4.2.2023.002>.
  53. D. Becker, P. Martínez-Garzón, T. Kılıç, M. Bohnhoff, Homogenized regional seismicity catalogue for the Marmara region, northwestern Turkey, for the time interval 2021–2023, GFZ Data Services (2025); <https://doi.org/10.5880/GFZ.ITSJ.2025.003>.
  54. Turkish National Seismic Network, (1990); <https://doi.org/10.7914/SN/TU>
  55. Kandilli Observatory Seismic Network, (1971); <https://doi.org/10.7914/SN/KO>
  56. PIRES Seismic Network, (2006); <https://doi.org/10.7914/SN/PZ>
  57. GONAF borehole seismic network (2013); <https://doi.org/10.14470/TS373432>.
  58. W. Zhu, G. C. Beroza, PhaseNet: A deep-neural-network-based seismic arrival-time picking method. *Geophys. J. Int.* **216**, 261–273 (2019).
  59. A. Lomax, A Reanalysis of the Hypocentral Location and Related Observations for the Great 1906 California Earthquake. *Bull. Seismol. Soc. Am.* **95**, 861–877 (2005). doi:10.1785/0120040141
  60. P. Martínez-Garzón, D. Becker, J. Jara, X. Chen, G. Kwiatek, M. Bohnhoff, The 2022 Mw 6.0 Gölyaka–Düzce earthquake: An example of a medium-sized earthquake in a fault zone early in its seismic cycle. *Solid Earth* **14**, 1103–1121 (2023).

[doi:10.5194/se-14-1103-2023](https://doi.org/10.5194/se-14-1103-2023)

61. S. R. Kotha, G. Weatherill, D. Bindi, F. Cotton, A regionally-adaptable ground-motion model for shallow crustal earthquakes in Europe. *Bull. Earthquake Eng.* **18**, 4091–4125 (2020). [doi:10.1007/s10518-020-00869-1](https://doi.org/10.1007/s10518-020-00869-1)
62. S. Wiemer, M. Wyss, Mapping the frequency-magnitude distribution in asperities: An improved technique to calculate recurrence times? *J. Geophys. Res.* **102**, 15115–15128 (1997). [doi:10.1029/97JB00726](https://doi.org/10.1029/97JB00726)
63. Y. Okada, Surface deformation due to shear and tensile faults in a half-space. *Bull. Seismol. Soc. Am.* **75**, 1135–1154 (1985). [doi:10.1785/BSSA0750041135](https://doi.org/10.1785/BSSA0750041135)
64. R. F. Kartal, F. T. Kadrioglu, T. Kılıç, An improved earthquake and moment tensor catalogues ( $M \geq 4.0$ ) for Anatolian region and its near vicinity (2013–2019). *Arab. J. Geosci.* **15**, 1632 (2022). [doi:10.1007/s12517-022-10933-6](https://doi.org/10.1007/s12517-022-10933-6)
65. J. Lin, R. S. Stein, Stress triggering in thrust and subduction earthquakes and stress interaction between the southern San Andreas and nearby thrust and strike-slip faults. *J. Geophys. Res. Solid Earth* **109**, B02303 (2004).
66. S. Toda, R. S. Stein, K. Richards-Dinger, S. B. Bozkurt, Forecasting the evolution of seismicity in southern California: Animations built on earthquake stress transfer. *J. Geophys. Res. Solid Earth* **110**, B05S16 (2005).

## ACKNOWLEDGMENTS

We thank the support from Oliver Fabisch to download event waveform data, and from Grzegorz Kwiatek to share in-house programs related to the b-positive calculations. We also thank Orhan Tatar, Aykut Akgun and Oliver Heidbach for helpful discussion related to the topics addressed here. **Funding:** P.M.G. and S.N.J. are funded by the ERC Starting Grant -101076119 (QUAKEHUNTER). X. C. received funding from the Deutsche Forschungs Gemeinschaft (DFG) in the frame of the proposal "Earthquake source characterization and directivity effects near Istanbul: Implications for seismic hazard". **Author contributions:** Conceptualization: PMG, GD, FC, MB. Methodology: XC, DB, RFK, ET. Investigation: SNJ, PMG, RFK, FTK, TK, YBZ. Visualization: JJ, SNJ, PMG, XC, ET. Funding acquisition: PMG, MB, FC. Project administration: MB, FC, PMG. Supervision: PMG, GD, MB, FC, YBZ. Writing – original draft: PMG, GD, MB, FC. Writing – review and editing: All authors. **Competing interests:** Authors declare that they have no competing interests. **Data and materials availability:** For the decade-long evolution of seismicity, we employ the catalog available in (52) previously covering from January 1st 2006 00:00 UTC until January 1st 2021. Here the seismicity catalog was updated until January 1st 2024 00:00 UTC is provided in (53). Waveform data used to analyze the 2025  $M_w$  6.2 and 2019  $M_w$  5.8 was acquired from (54–57). We employed the AFAD-DDA Earthquake Department online catalog from January 1st 2024 00:00 UTC until May 3rd 2025 15:00 UTC for the coordinates Longitude [27, 30], Latitude [40, 41] available from <https://deprem.afad.gov.tr/event-catalog>. Strong motion data was retrieved from the Turkish Accelerometric Database and Analysis System (AFAD-TADAS, <https://tadas.afad.gov.tr/login>). For estimation of the  $b$ -value, we employed MATLAB and Python codes based on (45). Single event earthquake localization was performed with version 7.0.0 of the NLloc software available at <http://alomax.free.fr/nlloc/> (last accessed on 11/09/2025). To assess the impact of these earthquakes on the regional stress distribution, the Coulomb 3.4 software was employed, which is available at <https://temblor.net/coulomb/> (last accessed on 11/09/2025). MATLAB, Python and Generic Mapping Tools were used for data processing and figure producing. All other data needed to evaluate the conclusions in the paper are present in the paper or the supplement. No samples or new materials were collected or generated for this study. **License information:** Copyright © 2025 the authors, some rights reserved; exclusive licensee American Association for the Advancement of Science. No claim to original US government works. <https://www.sciencemag.org/about/science-licenses-journal-article-reuse>

## SUPPLEMENTARY MATERIALS

[science.org/doi/10.1126/science.adz0072](https://science.org/doi/10.1126/science.adz0072)

Materials and Methods  
Figs. S1 to S6  
References (58–66)

14 May 2025; accepted 26 November 2025

Published online 11 December 2025

10.1126/science.adz0072

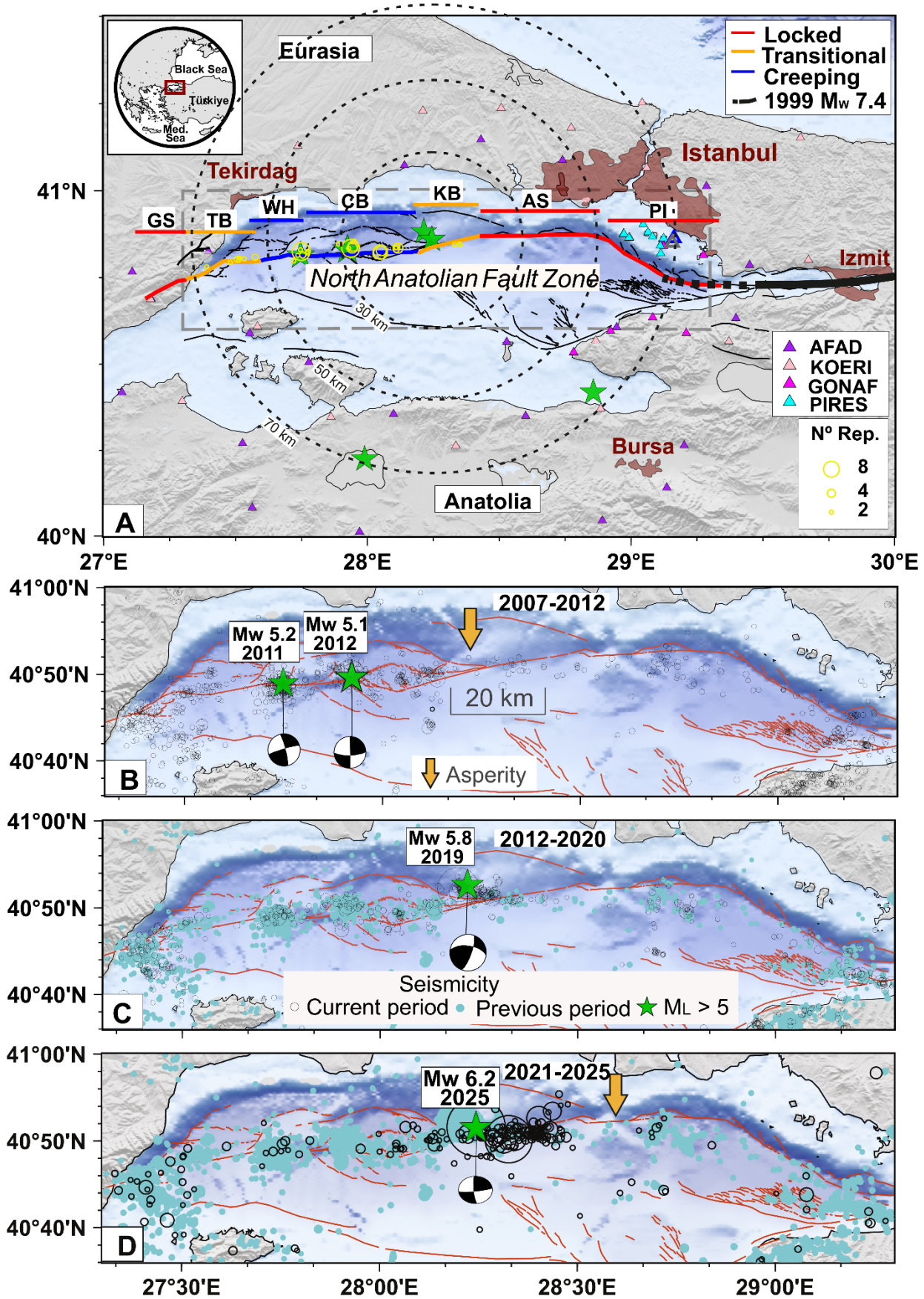


**Fig. 1. Segment fault behavior and seismicity evolution.** (A) Fault segments and their slip behavior along the Main Marmara fault (MMF), and  $M > 5$  earthquakes in the region from 2006. Blue, orange and red lines along the fault represent the creeping, transitional and locked segments, respectively. Open yellow circles represent the centroid of earthquake repeater clusters, with their size encoded with the number of repeaters in the clusters (22, ). Segment abbreviations are: GS: Ganos Segment; TB: Tekirdağ Basin; WH: Western High; CB: Central Basin; KB: Kumburgaz Basin; AS: Avcilar Segment; PI: Princes Islands. Upward triangles indicate seismic stations from different networks and agencies. The thick black line represents the rupture of the 1999  $M_w$  7.4 Izmit earthquake. Dashed circles mark distances from  $M_w$  6.2 epicenter. Gray box outlines the area shown in B-D. (B) Spatial distribution of  $M \geq 2.5$  earthquakes along the MMF during two different time periods (catalogs from (52, 53) and AFAD. (B) From January 1st 2007 to December 31st 2012, (C) From January 1st 2013 to December 31st 2020, (D) From January 1st 2021 to May 3rd 2025. Green stars represent the epicenters of the  $M > 5$  earthquakes during that time period. The two orange arrows indicate potential asperities discussed in the text. In (C, D), the blue dots represent the seismicity from the previous time period(s).

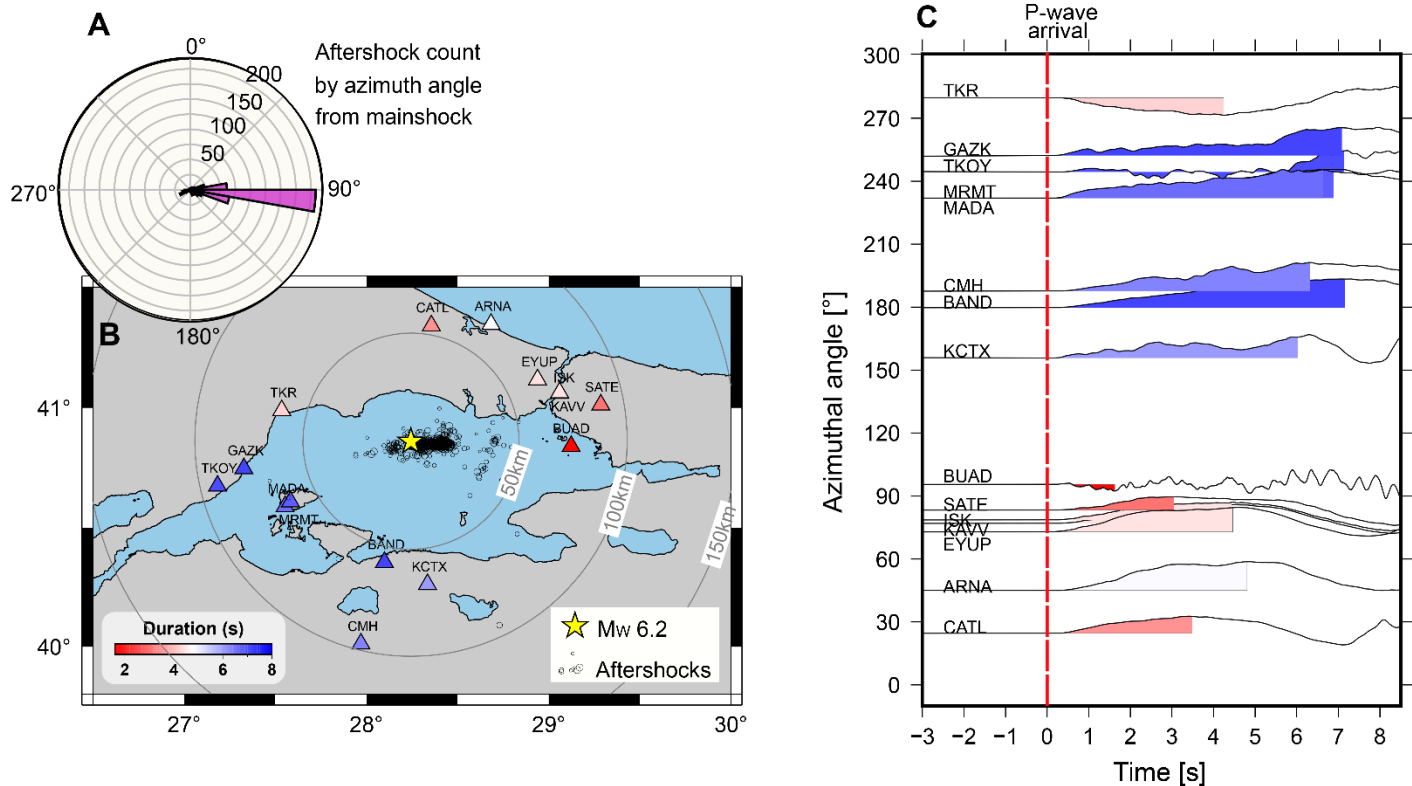


**Fig. 2. Eastward rupture propagation and aftershock sequence of the 2025 Mw 6.2 Marmara earthquake.** (A) Aftershock count by azimuth angle from the mainshock epicenter (1 week). (B) Epicenter of the Mw 6.2 earthquake and aftershock distribution (AFAD catalog). Upward triangles represent broadband seismometers at epicentral distances between 50 and 100 km and used in Panel C. Stations are color-encoded with the duration of the P-wave first pulses (see also C). (C) Normalized radial displacements and duration time of the P-wave first picks, with the area below color-encoded with the duration as in (A). Waveforms are aligned according to the P-wave first arrival.

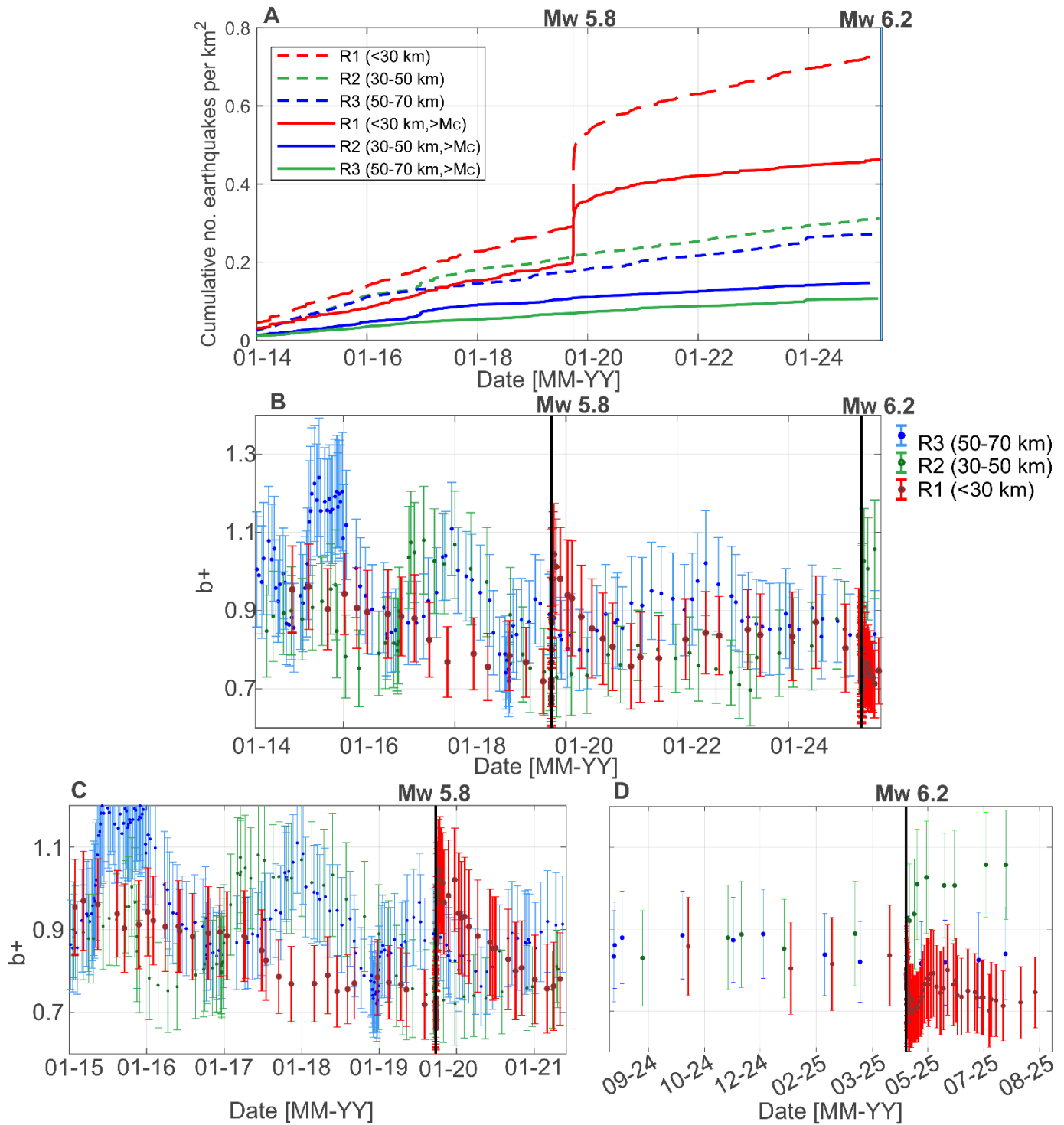


**Fig. 3. Seismicity and *b*-positive evolution at different distances from the M<sub>w</sub> 6.2 epicenter.** (A) Cumulative seismicity rates at R < 30 km (red), between 30 and 50 km (green), and between 50 and 70 km (blue). Dashed and solid lines represent the entire available catalogs and above magnitude of completeness (M<sub>c</sub>) 1.6, respectively. (B) Temporal evolution of the *b*-positive (*b*<sub>+</sub>) at different distances from the epicenter. The employed catalog covers from 1 January 2013 until 1 January 2024 (52, 53) and from 1 January 2024 to 18 August 2025 at 00:00 UTC (AFAD). Vertical bars represent 95% confidence intervals. (C and D) Similar to B but at half the step size and zoomed in on selected time periods around the 2019 M<sub>w</sub> 5.8 and 2025 M<sub>w</sub> 6.2 mainshocks..

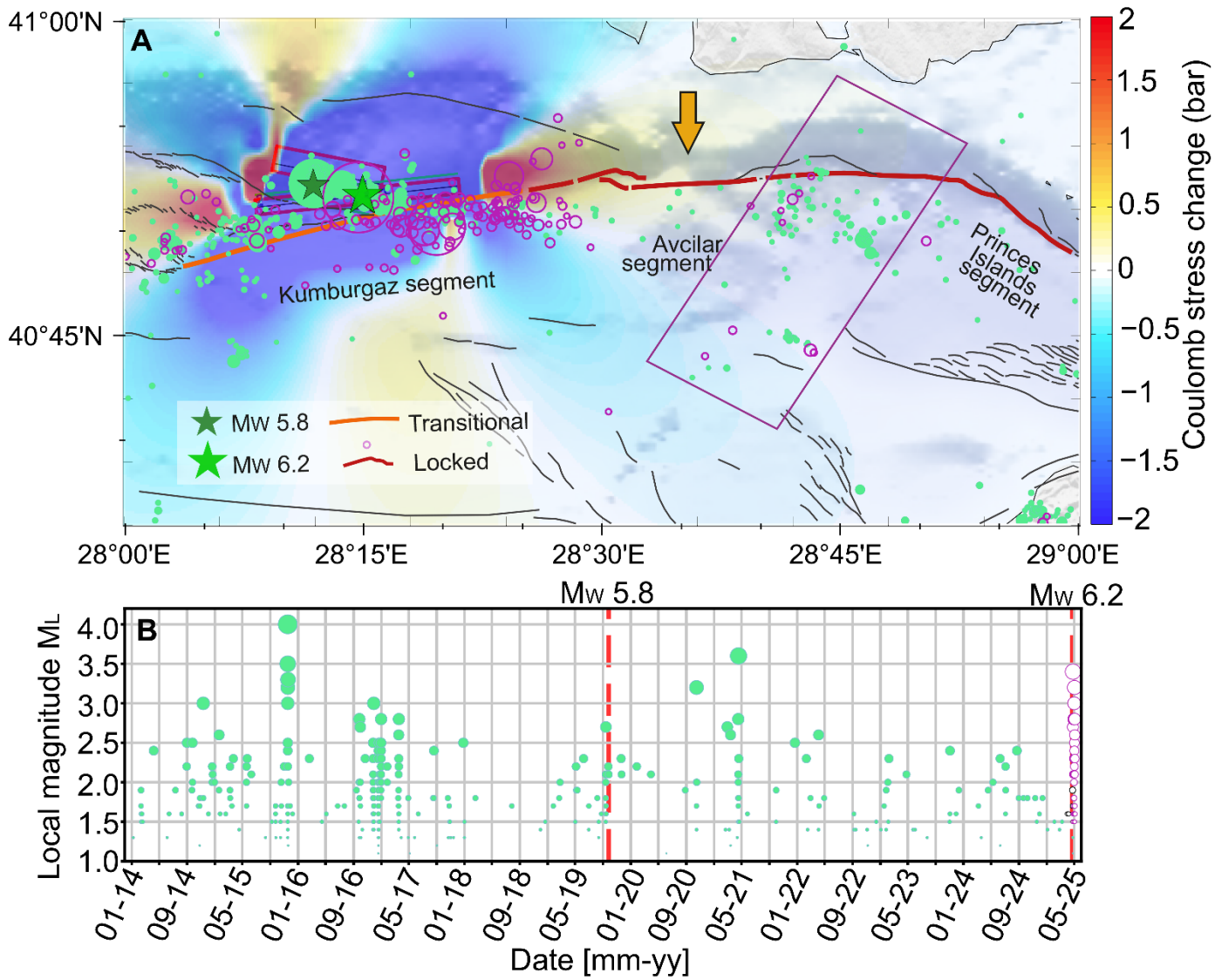


**Fig. 4. Stress transfer and fault dynamics in the Eastern Sea of Marmara.** (A) The aftershock sequence of the 2025 M<sub>W</sub> 6.2 earthquake as of 3 May 2025 (purple-edge circles size-encoded with magnitude, catalog from AFAD). Turquoise-filled circles represent the seismicity in the area from 2006–2023 (53). Superposed colors denote the static Coulomb stress transfer imposed by the 2019 M<sub>W</sub> 5.8 (epicenter shown with dark green star) and the 2025 M<sub>W</sub> 6.2 (epicenter shown with green star) on the MMF. The MMF is color-coded with the slip mode according to earthquake repeater analysis (22). Orange arrow marks the seismically silent portion here identified and suggested as a potential earthquake rupture area. The purple rectangle surrounds the seismically active area at the western end of the Princess Island seismic gap. (B) Magnitude (local magnitude M<sub>L</sub>)–time evolution of the seismicity from the purple rectangle in A.